

Photonic Mode Description of the Jaynes-Cummings Hamiltonian States

V. F. Maisi ^{1,*}

¹*NanoLund and Solid State Physics, Lund University, Box 118, 22100 Lund, Sweden*

(Dated: March 11, 2025)

Jaynes-Cummings Hamiltonian provides the elemental description of a two-level system interacting with a photonic mode. In this Article, we derive an expression for the transmission response via a photonic signal that describes the hybridized states as separate photonic modes. As a result, we obtain the effective input/output couplings and the internal losses of each mode. These set the decoherence rate of the hybridized states, and provide a simple description of the strength of the response signal, that we call "visibility", and its linewidth. In particular, the result allows us to describe a situation where the coherence increases significantly while the signal remains strongly visible in the response.

INTRODUCTION

Jaynes-Cummings (JC) Hamiltonian has a pivotal role in quantum physics. It is widely used to describe the light-matter interaction of atoms and optical cavities [1–6] as well as many solid-state quantum devices [7–13]. The JC Hamiltonian describes how a transition from one quantized state to another interacts coherently with a harmonic photonic mode, leading to the well-known Rabi splitting and Rabi oscillations in the strong-coupling regime when the coupling strength exceeds the losses in the system. The hybridization of the electronic and photonic states is also a generally known outcome of the coherent coupling, and the JC Hamiltonian predicts that the coherence of the hybridized states is a weighted sum of the electronic and photonic contributions.

One of the most common ways to measure systems following the JC Hamiltonian is to determine the transmission and reflection coefficient via couplings to the photonic mode. In this Article, we show that at low probe power - as usually used for characterizing the system under study - the eigenenergies of the hybridized states can be perceived analogously to the bare photonic resonator mode. We derive expressions for the coupling of the hybridized modes to the input/output lines as well as the internal losses related to the mode. Our results show that these are related to the bare coupling rates and losses weighted with the corresponding coefficients of the hybridized wavefunctions. The results constitute an intuitive picture of the modes consisting of a "visible" photonic part that interacts with the input/output lines and a "hidden" electronic part that does not connect directly to the probing signals. We then consider two illustrative cases: I) a case where the electronic system is as coherent or less coherent than the photonic one, and leads to the usually observed weakening of the transmission and reflection signal at decreasing hybridization; and II) a case where the electronic state is more coherent and gives rise to measurement signal that remains strong while the linewidth of the mode sharpens. The intuitive picture describes these cases in terms of changes in the

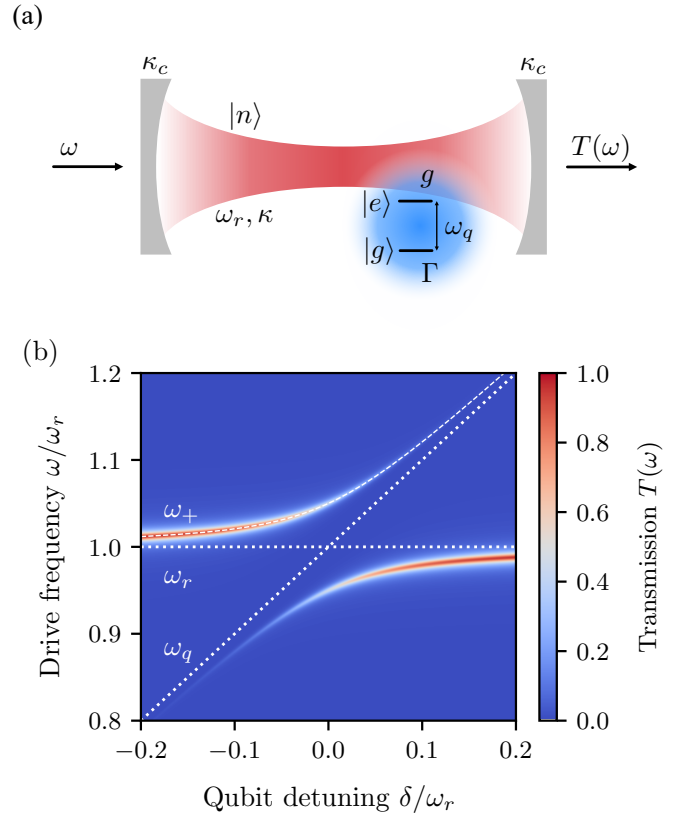


FIG. 1. (a) Elements of the considered JC system. A photonic mode (in red) with photon states $|n\rangle$, resonance frequency ω_r , coupling κ_c to the input and output port, and total photon loss rate κ . An electronic two-level system with states $|g\rangle$ and $|e\rangle$, energy ω_q , total decoherence rate Γ , and coupling g to the photonic mode. The transmission $T(\omega)$ is measured as a function of the frequency ω of the input tone. (b) The transmission $T(\omega)$ of Eq. (2) as a function of the drive frequency ω and qubit detuning $\delta = \omega_q - \omega_r$. The other parameter values are $\kappa_c = 5 \cdot 10^{-3} \omega_r$, $\kappa = 2 \kappa_c$ (i.e. no internal losses), $g = 0.05 \omega_r$ and $\Gamma = 10^{-2} \omega_r$.

effective input/output coupling and the internal losses of the mode. Therefore, it provides a simple and useful tool for understanding the features seen in the experi-

mental response. For completeness, we consider also the strong dephasing case. In this limit, the response consists of only one mode close to the bare resonator frequency. The two-level system gives rise to additional loss and a weak dispersive shift only.

THE JC SYSTEM CONSIDERED

Figure 1 (a) presents the system considered. It is among the most commonly used setups for studying coherent light-matter interactions. A photonic mode in red with resonance frequency ω_r is defined in a resonator structure. It couples to an input and output port with couplings κ_c . The linewidth and therefore also the decoherence rate, κ of this mode are set by the sum of these two couplings plus any additional photon losses. The response of the system is determined by measuring the transmission coefficient $T(\omega)$ for a weak input drive signal at frequency ω . With the weak drive, the photon number states $|n\rangle$ are limited to the lowest two states $|0\rangle$ and $|1\rangle$.

The JC Hamiltonian describes the interaction of a two-level system with this photon mode [2, 14, 15]. The two-level system, i.e. a qubit, is shown in blue in Fig. 1 (a). It has an energy difference ω_q between the ground state $|g\rangle$ and the excited state $|e\rangle$, and interacts with the photon mode with a coupling rate g . The decoherence rate of the two-level system is denoted by Γ . The JC Hamiltonian is then

$$\hat{H} = \omega_r \hat{a}^\dagger \hat{a} + \omega_q |e\rangle \langle e| + g(\hat{a} \hat{\sigma}^+ + \hat{a}^\dagger \hat{\sigma}^-), \quad (1)$$

where \hat{a}^\dagger and \hat{a} are the photon creation and annihilation operators respectively, and $\hat{\sigma}^+ = |e\rangle \langle g|$ and $\hat{\sigma}^- = |g\rangle \langle e|$ similarly for the two-level system. Here the energy reference is chosen so that the lowest state $|0\rangle \otimes |g\rangle = |0g\rangle$ is at zero energy. With this choice, the higher energy eigenenergies yield directly the transition energies from the ground state to the corresponding state visible in $T(\omega)$. By employing further input-output theory results in the weak input drive limit the transmission [8, 16, 17]

as

$$T(\omega) = |\kappa_c A(\omega)|^2, \quad (2)$$

where

$$A(\omega) = \frac{\Gamma/2 - i(\omega - \omega_q)}{[\kappa/2 - i(\omega - \omega_r)][\Gamma/2 - i(\omega - \omega_q)] + g^2}. \quad (3)$$

Figure 1 (b) shows the resulting transmission for a typical case in the strong-coupling regime, $g > \Gamma, \kappa$ as a function of input drive frequency ω and qubit detuning $\delta = \omega_q - \omega_r$. At large detuning $|\delta| \gg g$, the eigenstates of the system are close to the bare states $|n\rangle \otimes |q\rangle = |nq\rangle$ with the photon number $n = 0, 1, \dots$, and the qubit state $q = g, e$, and only the $|0\rangle \leftrightarrow |1\rangle$ transition is visible in the response at $\omega \approx \omega_r$. For small detuning, the states hybridize and show the Rabi-split avoided crossing. As well known in the field, the lowest eigenenergies are obtained by diagonalizing the JC Hamiltonian in the $|0e\rangle - |1g\rangle$ basis resulting in

$$\omega_\pm = (\omega_q + \omega_r)/2 \pm \Omega/2, \quad (4)$$

where $\Omega = \sqrt{\delta^2 + 4g^2}$. As seen in the figure, the transmission has strong resonant response at these energies. The corresponding eigenstates are

$$|\psi_\pm\rangle = c_\pm |0e\rangle \pm c_\mp |1g\rangle, \quad (5)$$

where $c_\pm = \sqrt{(1 \pm \delta/\Omega)/2}$. This expression turns out to be useful in the following and is equivalent to the more frequently used expressions $c_+ = \cos(\phi/2)$ and $c_- = \sin(\phi/2)$ with the so-called mixing angle $\phi = \arctan(2g/\delta)$ [2, 14, 15].

MODES IN THE STRONG-COUPLING CASE

To proceed, we limit our consideration to the strong-coupling case for which $\Gamma, \kappa < g$. In this case, the eigenenergies are well separated from each other, and their response around the frequencies ω_\pm is far away from ω_q . In the following, we consider the response $T(\omega)$ nearby these modes allowing us to approximate $\Gamma/2 - i(\omega - \omega_q) = i(\omega - \omega_q) = i(\omega_\pm - \omega_q)$ in the nominator of Eq. (3). With this, we obtain

$$A(\omega) = \frac{\omega_\pm - \omega_q}{\kappa/2(\omega - \omega_q) + \Gamma/2(\omega - \omega_r) - i(\omega - \omega_+) (\omega - \omega_-)} = \frac{\omega_\pm - \omega_q}{\kappa/2(\omega_\pm - \omega_q) + \Gamma/2(\omega_\pm - \omega_r) \mp i\Omega(\omega - \omega_\pm)}, \quad (6)$$

where the upper choice is for the ω_+ mode around $\omega = \omega_+$ and the lower one for the ω_- mode around $\omega = \omega_-$. Here we have neglected the term $\kappa\Gamma/4 \ll g^2$ which gives rise

to a small shift to the resonance frequencies in form of a renormalization of g . Next we note that the energy differences are connected to the hybridization of the photonic

and electronic states via the wave function coefficients c_{\pm} as $\omega_{\pm} - \omega_r = \pm\Omega |c_{\pm}|^2$ and $\omega_{\pm} - \omega_q = \pm\Omega |c_{\mp}|^2$. Therefore, we obtain finally with Eqs. (2) and (6) the transmission coefficient of the system as

$$T(\omega) = \frac{\kappa_{c_{\pm}}^2}{(\kappa_{\pm}/2)^2 + (\omega - \omega_{\pm})^2}, \quad (7)$$

where $\kappa_{c_{\pm}} = \kappa_c |c_{\mp}|^2$ and $\kappa_{\pm} = \kappa |c_{\mp}|^2 + \Gamma |c_{\pm}|^2$. Equation (7) is a Lorentzian and forms the main result of this Article. It has identical structure as the transmission of the bare resonator has with $T(\omega) = \kappa_c^2 / ((\kappa/2)^2 + (\omega - \omega_r)^2)$, see e.g. Refs. 18, 19. In Eq. (7) each of the two states $|\psi_{\pm}\rangle$ of Eq. (5) gives rise to a Lorentzian response with the $|0g\rangle \leftrightarrow |\psi_{\pm}\rangle$ transition at resonance frequency ω_{\pm} . The coupling of these modes are given by the original photonic coupling κ_c scaled with the wavefunction weight $|c_{\mp}|^2$ of the bare photonic excitation component $|1g\rangle$ of Eq. (5). Similarly, the linewidth of the mode κ_{\pm} , i.e. total decoherence rate of the mode, is a sum of the photonic contribution with the rate κ and the same photonic weight, and the corresponding electronic contribution with the rate Γ and the corresponding wavefunction weight $|c_{\pm}|^2$ of the bare electronic excitation component $|0e\rangle$. With these results, we get for example in the resonant case $\delta = 0$ the well-known result $\kappa_{\pm} = (\kappa + \Gamma)/2$, i.e. that the decoherence rate for the fully hybridized states is the average of the electronic and photonic decoherence rate [8, 13]. The couplings of the modes derived here allows to obtain further insights to the interaction dynamics, and connects the visibility of the hybridized states and the coherence of the electronic system together as we discuss next.

In Fig. 1 (b), the photonic and electronic coherence is chosen equal, $\kappa = \Gamma$, such that the decoherence rate, i.e. the effective internal losses, of the hybridized states remains constant $\kappa_{\pm} = \kappa$. The visibility of the bare photonic mode then decreases as the state hybridizes and turns more into the electronic one. The reduction of the visibility is because the input/output coupling reduces the larger the electronic part of the state is. The bare photonic state has the highest transmission of $T(\omega_{\pm}) = 4\kappa_c^2/\kappa^2$. As the states hybridize and obtain larger and larger electronic fraction, the transmission reduces as $T(\omega_{\pm}) = 4\kappa_c^2 |c_{\mp}|^4 / \kappa^2$. Figure 2 depicts another interesting case. Here all the other parameter values are the same except the decoherence rate Γ of electronic state, which is reduced to have $\Gamma \ll \kappa, \kappa_c$, such that the electronic system is more coherent than the photonic one. In this case, the non-hybridized photonic states have still the high transmission of $T(\omega_{\pm}) = 4\kappa_c^2/\kappa^2$. However, as these states hybridize with the electronic one, the transmission stays high, as see in Fig. 2 (a) for the states close to ω_q , and in the corresponding line cuts of Fig. 2 (b). At the same time, the Lorentzian becomes sharper with a smaller linewidth. These effects can be again under-

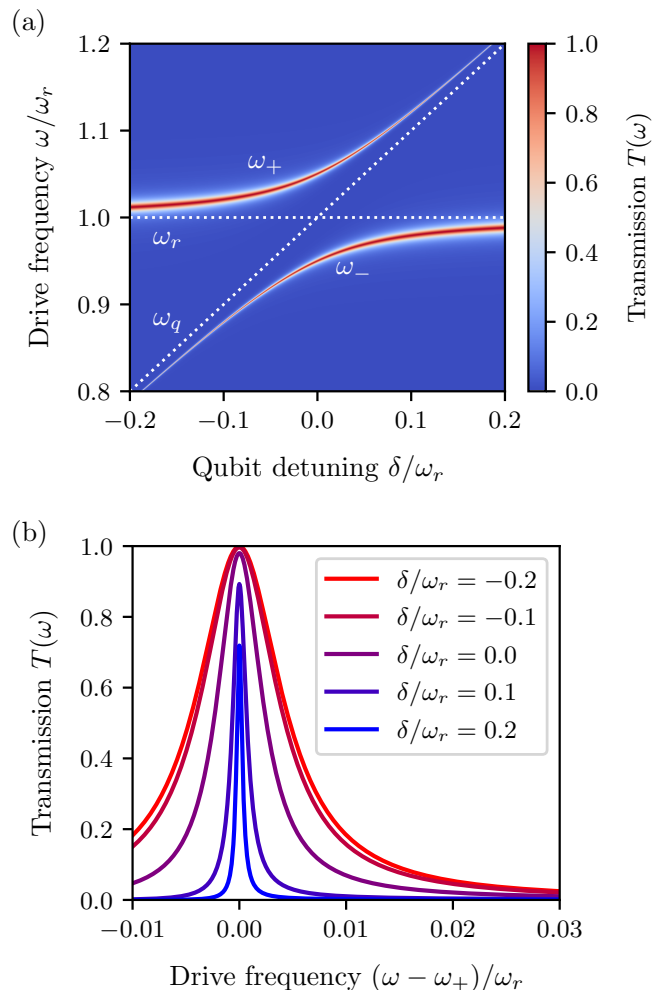


FIG. 2. (a) The transmission $T(\omega)$ of Eq. (2) for a high-coherence two-level system with $\kappa_c = 5 \cdot 10^{-3} \omega_r$, $\kappa = 2 \kappa_c$, $g = 0.05 \omega_r$ and $\Gamma = 10^{-4} \omega_r$. (b) The transmission $T(\omega)$ plotted as a function of drive frequency ω around the mode at frequency ω_+ . The red data is at $\delta < 0$ where the mode is predominantly photonic and the blue one at $\delta > 0$ where the mode is predominantly electronic. For this case, the transmission still stays close to unity while the linewidth decreases significantly.

stood with the couplings of Eq. (7). For small Γ , both the $\kappa_{c_{\pm}}$ and κ_{\pm} scale proportional to $|c_{\mp}|^2$. Therefore both the coupling and the total decoherence rate reduce in concert leading to higher coherence and remaining high transmission despite the state becoming more electronic.

Figure 3 summarizes the above findings by presenting the maximum transmission $T(\omega_+)$ and the linewidth κ_+ for the two cases. The dots show the transmission and linewidth extracted directly from Eq. (2), and the lines the corresponding values based on the Lorentzian of Eq. (7). Blue data is for the $\Gamma = \kappa$ case and red one for the $\Gamma \ll \kappa, \kappa_c$. We see that the Lorentzian approximation catches the main features of the data: The

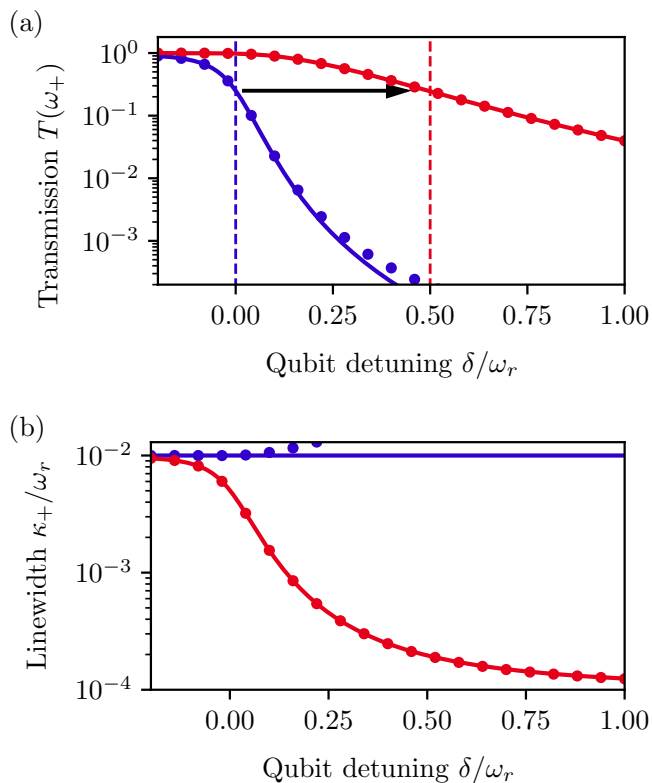


FIG. 3. The maximum transmission $T(\omega_+)$, panel (a), and linewidth κ_+ , panel (b), for the mode ω_+ for different detunings. The blue data is for the case in Fig. 1 and the red data for the Fig. 2 case. The dots are determined from the full response of Eq. (2), while the lines show the result of Eq. (7). The results for the mode ω_- are the same with mirroring $\delta \mapsto -\delta$. The dashed lines denote the condition $\kappa|c_{\mp}|^2 = \Gamma|c_{\pm}|^2$ where the linewidth has equal contributions from the photonic and electronic part. At this condition, the transmission is reduced by a factor of 4.

maximum transmission $T(\omega_+)$ starts at a close-to-unity value and reduces at around $\delta \approx 0$ for the blue data of the $\Gamma = \kappa$ case as the bare resonator state hybridizes significantly with the electronic contribution. At the same time, the total linewidth stays approximately constant. At large positive δ , the state becomes predominantly electronic like and the transmission is suppressed. In this case, the precise response deviates from the prediction of Eq. (7) since the tails of the much stronger $|0g\rangle \leftrightarrow |\psi_-\rangle$ transition contribute significantly at around ω_+ . This leads to larger transmission $T(\omega_+)$ and increased estimated linewidth in the figure. This regime is, however not particularly relevant as the response is already suppressed and typically not resolvable in the experiments any more [9, 11, 13].

The red points and lines of Fig. 3 repeat the summary for the coherent case of Fig. 2. Again, the solid lines of Eq. (7) predict the response accurately. Now, instead of the transmission $T(\omega_+)$ decreasing at around $\delta \approx 0$,

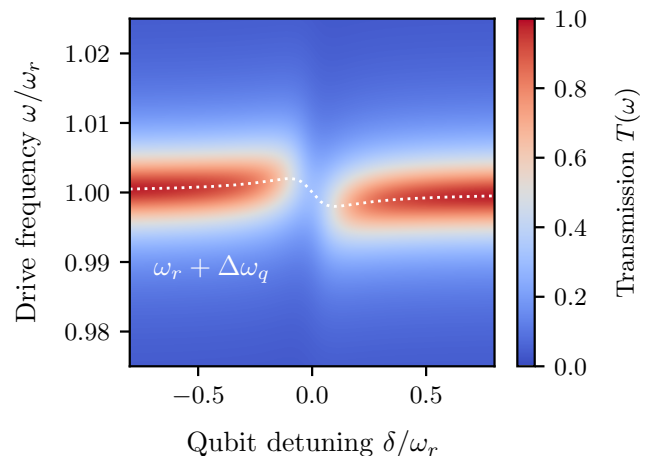


FIG. 4. The transmission $T(\omega)$ of Eq. (2) in the weak coupling limit with $\kappa_c = 5 \cdot 10^{-3} \omega_r$, $\kappa = 2 \kappa_c$, $g = 0.02 \omega_r$ and $\Gamma = 0.2 \omega_r$. The white dashed line indicates the shifted resonance frequency $\omega_r + \Delta\omega_q$ of Eq. (10).

rather the linewidth starts decreasing and the resonance sharpens here as the hybridization with the electronic part sets in. The high transmission coefficient and sharpening of the response continue until $\kappa_+ \approx \Gamma$. After this point, the linewidth saturates towards a constant value of Γ and the transmission starts reducing analogous to the less coherent case of the blue data. The onset point for the reduction of $T(\omega_+)$ shifts from the $\delta \approx 0$ point to the condition $\kappa|c_{\mp}|^2 = \Gamma|c_{\pm}|^2$, i.e. to the point where the decoherence of the photonic part has equal contribution to κ_{\pm} as the electronic contribution. Under this condition, the ratio $\kappa_{\pm}/\kappa_{e\pm}$ doubles and leads to a factor of 4 reduction in $T(\omega_{\pm})$, see Eq. (7). With the assumption $\Gamma \ll \kappa$, this takes place at $\delta = \sqrt{\kappa/\Gamma}g$. For the presented data, we obtain $\delta/\omega_r = 0.5$ as indicated with the black arrow in Fig. 3 (a).

RESONATOR MODE IN THE WEAK-COUPLING LIMIT

When the dephasing rate Γ exceeds the coupling g , the resonator response consists of only one mode near the bare resonator frequency [20] as shown in Fig. 4. With $\Gamma > g$, we can rewrite Eq. (3) as

$$A(\omega) = \frac{1}{[\kappa/2 - i(\omega - \omega_r)] + g\chi}, \quad (8)$$

where $\chi = g/[\Gamma/2 - i(\omega - \omega_q)]$ is the electronic susceptibility of the two-level system [12]. For the considered case, $\Gamma > g$ the susceptibility is small, i.e. $|\chi|/2 < 1$. We can then proceed by considering the response close to the bare resonator frequency, $\omega \approx \omega_r$, and determine the

real and imaginary part of the χ . These are the added dissipation κ_q and dispersive shift $\Delta\omega_q$ that read as

$$\kappa_q = \frac{4g^2}{\Gamma} \frac{1}{1 + (2\delta/\Gamma)^2}, \quad (9)$$

and

$$\Delta\omega_q = -\frac{2g^2}{\Gamma} \frac{2\delta/\Gamma}{1 + (2\delta/\Gamma)^2}. \quad (10)$$

The response function $A(\omega)$ reads then as

$$A(\omega) = \frac{1}{(\kappa + \kappa_q)/2 - i(\omega - \omega_r - \Delta\omega_q)}. \quad (11)$$

This equation is the bare resonator Lorentzian response with added loss κ_q and resonance frequency shift $\Delta\omega_q$. It reproduces the full response of Fig. 4 with vanishingly small differences ($|\Delta T(\omega)| < 0.02$). We can further see from Eq. (9) that the maximum loss $\kappa_q = 4g^2/\Gamma$ is obtained at zero detuning $\delta = 0$ in line with the double quantum loss used in Ref. 21. At finite detuning, we have the additional coefficient $1/(1 + (2\delta/\Gamma)^2)$. This prefactor is that of the Purcell effect, i.e. that the losses increase when an additional lossy resonance mode is brought close in detuning [22]. Note that here we consider the losses added by the two-level system to the resonator, which is the opposite to Ref. 22 where the losses of the resonator influencing the qubit coherence was considered. The effect works the same way in both directions. The dispersive shift of Eq. (10) has a maximal value of $\Delta\omega_q = \pm g^2/\Gamma$ for $\delta = \pm\Gamma/2$. For $\delta = 0$, the dispersive shift vanishes.

SUMMARY

In summary, we derived the Lorentzian transmission lineshape for the lowest modes of the JC Hamiltonian and discussed two exemplary cases, one with lower coherence for the electronic state and another one with higher coherence. The Lorentzian response has an analogous form as the bare resonator response with input and output coupling and internal losses set by weighted averages of the hybridized modes. These simple intuitive relations provide a useful tool to determine the underlying coherence of the electronic state based on the 'visibility' $T(\omega_{\pm})$ and the linewidth κ_{\pm} of the hybridized states. This mapping allows for treating further states hybridizing to these ones iteratively. If another two-level system interacts with the system considered here - either via the photonic mode or via the electronic one, the Lorentzian mode at either frequency ω_{\pm} can be treated as the 'bare' system with which the next two-level system hybridizes further. This iterative process is expected to work analogously as long as the other mode ω_{\mp} stays sufficiently

far away from the response arising from the second hybridization. Such a case can be realized for example at $\delta \gtrsim \pm 2g$, where the first hybridization is already taking place partially while keeping the second state sufficiently detuned.

ACKNOWLEDGEMENTS

We thank Pierre Glidic for performing the experiments with double quantum dot states interacting with a high impedance microwave resonator. These measurement results initiated the consideration on what determines the visibility and linewidth of an electronic state in the photonic response. We thank the European Union (ERC, QPHOTON, 101087343) and NanoLund for financial support. Views and opinions expressed are however those of the author(s) only and do not necessarily reflect those of the European Union or the European Research Council Executive Agency. Neither the European Union nor the granting authority can be held responsible for them.

* ville.maisi@ftf.lth.se

- [1] H. J. Kimble, Strong interactions of single atoms and photons in cavity qed, *Phys. Scr.* **1998**, 127 (1998).
- [2] S. Haroche and J.-M. Raimond, *Exploring the Quantum: Atoms, Cavities, and Photons* (Oxford University Press, 2006).
- [3] R. J. Thompson, G. Rempe, and H. J. Kimble, Observation of normal-mode splitting for an atom in an optical cavity, *Phys. Rev. Lett.* **68**, 1132 (1992).
- [4] M. Brune, F. Schmidt-Kaler, A. Maali, J. Dreyer, E. Hagley, J. M. Raimond, and S. Haroche, Quantum Rabi Oscillation: A Direct Test of Field Quantization in a Cavity, *Phys. Rev. Lett.* **76**, 1800 (1996).
- [5] J. P. Reithmaier, G. Sek, A. Löffler, C. Hofmann, S. Kuhn, S. Reitzenstein, L. V. Keldysh, V. D. Kulakovskii, T. L. Reinecke, and A. Forchel, Strong coupling in a single quantum dot–semiconductor microcavity system, *Nature* **432**, 197 (2004).
- [6] T. Yoshie, A. Scherer, J. Hendrickson, G. Khitrova, H. M. Gibbs, G. Rupper, C. Ell, O. B. Shchekin, and D. G. Deppe, Vacuum Rabi splitting with a single quantum dot in a photonic crystal nanocavity, *Nature* **432**, 200 (2004).
- [7] A. A. Clerk, K. W. Lehnert, P. Bertet, J. R. Petta, and Y. Nakamura, Hybrid quantum systems with circuit quantum electrodynamics, *Nature Phys.* **16**, 257 (2020).
- [8] A. Blais, A. L. Grimsmo, S. M. Girvin, and A. Wallraff, Circuit quantum electrodynamics, *Rev. Mod. Phys.* **93**, 025005 (2021).
- [9] A. Wallraff, D. I. Schuster, A. Blais, L. Frunzio, R.-S. Huang, J. Majer, S. Kumar, S. M. Girvin, and R. J. Schoelkopf, Strong coupling of a single photon to a superconducting qubit using circuit quantum electrodynamics, *Nature* **431**, 162 (2004).

- [10] X. Mi, J. V. Cady, D. M. Zajac, P. W. Deelman, and J. R. Petta, Strong coupling of a single electron in silicon to a microwave photon, *Science* **355**, 156 (2017).
- [11] A. Stockklauser, P. Scarlino, J. V. Koski, S. Gasparinetti, C. K. Andersen, C. Reichl, W. Wegscheider, T. Ihn, K. Ensslin, and A. Wallraff, Strong Coupling Cavity QED with Gate-Defined Double Quantum Dots Enabled by a High Impedance Resonator, *Phys. Rev. X* **7**, 011030 (2017).
- [12] G. Burkard, M. J. Gullans, X. Mi, and J. R. Petta, Superconductor–semiconductor hybrid-circuit quantum electrodynamics, *Nature Rev. Phys.* **2**, 129 (2020).
- [13] A. Ranni, S. Haldar, H. Havir, S. Lehmann, P. Scarlino, A. Baumgartner, C. Schönenberger, C. Thelander, K. A. Dick, P. P. Potts, and V. F. Maisi, Decoherence in a crystal-phase defined double quantum dot charge qubit strongly coupled to a high-impedance resonator, *Phys. Rev. Res.* **6**, 043134 (2024).
- [14] A. Blais, R.-S. Huang, A. Wallraff, S. M. Girvin, and R. J. Schoelkopf, Cavity quantum electrodynamics for superconducting electrical circuits: An architecture for quantum computation, *Phys. Rev. A* **69**, 062320 (2004).
- [15] L. Childress, A. S. Sørensen, and M. D. Lukin, Mesoscopic cavity quantum electrodynamics with quantum dots, *Phys. Rev. A* **69**, 042302 (2004).
- [16] S. M. Girvin, Circuit QED: superconducting qubits coupled to microwave photons, in *Quantum Machines: Measurement and Control of Engineered Quantum Systems: Lecture Notes of the Les Houches Summer School: Volume 96, July 2011* (Oxford University Press, 2014) pp. 113–256.
- [17] J. H. Ungerer, A. Pally, A. Kononov, S. Lehmann, J. Ridderbos, P. P. Potts, C. Thelander, K. A. Dick, V. F. Maisi, P. Scarlino, A. Baumgartner, and C. Schönenberger, Strong coupling between a microwave photon and a singlet-triplet qubit, *Nature Commun.* **15**, 1068 (2024).
- [18] M. Göppl, A. Fragner, M. Baur, R. Bianchetti, S. Filipp, J. M. Fink, P. J. Leek, G. Puebla, L. Steffen, and A. Wallraff, Coplanar waveguide resonators for circuit quantum electrodynamics, *J. Appl. Phys.* **104**, 113904 (2008).
- [19] A. Ranni, H. Havir, S. Haldar, and V. F. Maisi, High impedance josephson junction resonators in the transmission line geometry, *Appl. Phys. Lett.* **123**, 114002 (2023).
- [20] T. Frey, P. J. Leek, M. Beck, A. Blais, T. Ihn, K. Ensslin, and A. Wallraff, Dipole coupling of a double quantum dot to a microwave resonator, *Phys. Rev. Lett.* **108**, 046807 (2012).
- [21] W. Khan, P. P. Potts, S. Lehmann, C. Thelander, K. A. Dick, P. Samuelsson, and V. F. Maisi, Efficient and continuous microwave photoconversion in hybrid cavity-semiconductor nanowire double quantum dot diodes, *Nature Commun.* **12**, 5130 (2021).
- [22] A. A. Houck, J. A. Schreier, B. R. Johnson, J. M. Chow, J. Koch, J. M. Gambetta, D. I. Schuster, L. Frunzio, M. H. Devoret, S. M. Girvin, and R. J. Schoelkopf, Controlling the spontaneous emission of a superconducting transmon qubit, *Phys. Rev. Lett.* **101**, 080502 (2008).